Plasma Sci. Technol. **25** (2023) 045405 (9pp) https://doi.org/10.1088/2058-6272/aca5f3

Generation of atmospheric pressure air diffuse discharge plasma in oxygen enriched working gas with floating electrode

Min ZHANG (张敏)[1,2], **Yunhu LIU** (刘云虎)[1,*], **Yao LI** (李瑶)[2], **Shuqi LI** (李淑琪)[1,2], **Hao YUAN** (袁皓)[2], **Jianping LIANG** (梁建平)[2], **Xiongfeng ZHOU** (周雄峰)[2] **and Dezheng YANG** (杨德正)[2,3,*]

[1] School of Sciences, Shihezi University, Shihezi 832003, People's Republic of China
[2] Key Laboratory of Materials Modification by Laser, Ion and Electron Beams, Dalian University of Technology, Ministry of Education, Dalian 116024, People's Republic of China
[3] Key Laboratory of Environmental Monitoring and Pollutant Control of Xinjiang Bingtuan, Shihezi University, Shihezi 832003, People's Republic of China

E-mail: yangdz@dlut.edu.cn and liuyh@shzu.edu.cn

Received 15 September 2022, revised 14 November 2022
Accepted for publication 24 November 2022
Published 8 February 2023

Abstract

In this work, a floating electrode is employed to generate a stable large-area diffuse discharge plasma under an open oxygen-rich environment. The discharge image and the optical emission spectra of the N_2(C-B), N_2^+(B-X), N_2(B-A), and O(3p–3s, 777 nm) are measured to analyze the morphological and optical characteristics of the discharge. The effects of applied voltage, gas flow rate, and electrode gap on the reactive species, vibrational temperature and rotational temperature are investigated, and the discharge mode is discussed by simulating the electrostatic field before the breakdown. It is found that the changes of applied voltage and electrode gap causes the transition of the discharge modes among corona mode, diffuse discharge mode and spark mode. It is shown that the floating electrode can inhibit the transition from discharge to spark mode to a certain extent, which is conducive to maintaining the stability of discharge. As is vividly illustrated in this study, the increase of applied voltage or the decrease of electrode gap contributes to the generation of more active particles, such as N_2(C) and N_2^+(B). Furthermore, the Joule heating effect becomes more evident with the increased applied voltage when the electrode gap is 15 and 20 mm. Moreover, as the applied voltage increases, the vibrational temperature increases at the electrode gap of 25 mm.

Keywords: floating electrode, optical emission spectra, vibrational temperature, rotational temperature

(Some figures may appear in colour only in the online journal)

1. Introduction

Non-thermal plasma, which is known as high electron temperature and low gas temperature, is widely used in biomedicine [1–3], food processing [4–6], material surface modification [7–9], chemical industry [10, 11] and other fields. Most of those applications rely on reactive oxygen species (ROS) and require uniform discharge (e.g. glow). Producing a high density of ROS (e.g. OH, O), which can participate in the reactions with the target material, is of great value [12, 13]. The atmospheric pressure discharge (especially in the bare electrode structure) is easily transformed into the filament, spark discharge, or arc discharge [14–17], which will damage the sample and limit the application who is sensitive to discharge uniformity. Therefore, obtaining a diffuse or uniform discharge in atmospheric air is a challenge attracting countless scientists.

* Authors to whom any correspondence should be addressed.

The key to obtain a uniform or diffuse discharge is to prevent the transition from glow or uniform to the filament, spark discharge, arc discharge, etc. In recent years, researchers have used the forms of designing excitation power supply, adjusting discharge parameters and optimizing electrode structure to generate diffuse discharge plasma. They have carried out a large number of experimental and theoretical studies. Zhang *et al* demonstrated that a smaller pulse peak voltage or discharge gap is more conducive to improving the discharge uniformity of nanosecond-pulse discharge [18]. The studies of Shi *et al* show that compared with naked electrodes, the dielectric insulation of electrodes is conducive to the stability of radio-frequency glow, and the reason is that the dielectric barrier can prevent the infinite growth of discharge current and thus reduce the tendency of the glow-to-spark transition (GST) [19–21]. In addition, GST can also be regulated by specially designed electrode structures. Kanazawa *et al* proposed to use different grounding electrodes and nozzle shapes to control the DC corona discharge mode in atmospheric air [22].

To generate diffuse discharge, various floating electrodes (FEs) which are isolated (voltage-free, ungrounded) conductors are added to the electrode configuration [23, 24]. The FE added between the high-voltage electrode and the ground electrode will form an equipotential body, and the consequential change of the original electric field distribution affects the discharge operation. The preferred electric field can be obtained by changing the shape and position of FE. In recent years, the FE structure has been used to stabilize the discharge plasma and increase the length of the plasma feather, so as to improve the performance of the plasma source. Deepak *et al* show that the ring or helix FE is beneficial to restrict the transition of glow to arc and effectively increase the length of the plasma jet [25, 26]. A plasma reactor with a plate FE, which has a solid metal top half and a metallic foam bottom half, designed by Zhu *et al,* increases the volume of plasma light-emitting area and improves the efficiency of hydrogen production [27].

In this paper, in order to overcome the discharge instability under the bare electrode structure, we developed a cap FE configuration to generate a stable diffuse discharge in a large electrode gap using oxygen enriched working gas under the excitation of a DC power supply. The formation mechanism of the diffuse discharge plasma with FE is analyzed, and the effects of FE on breakdown voltage and GST voltage are studied. In addition, emission spectra of the active particles and discharge images are recorded to discuss the discharge characteristics, active species, and gas temperature.

2. Experimental setup

The experimental setup is shown in figure 1(a) and the electrode structure of the plasma reactor is detailed in figure 1(b). The experimental setup is composed of a DC power supply, a discharge reactor, a gas inlet system and an optical detection system. The DC power supply can provide a voltage range of 0–60 kV and this work uses negative polarity

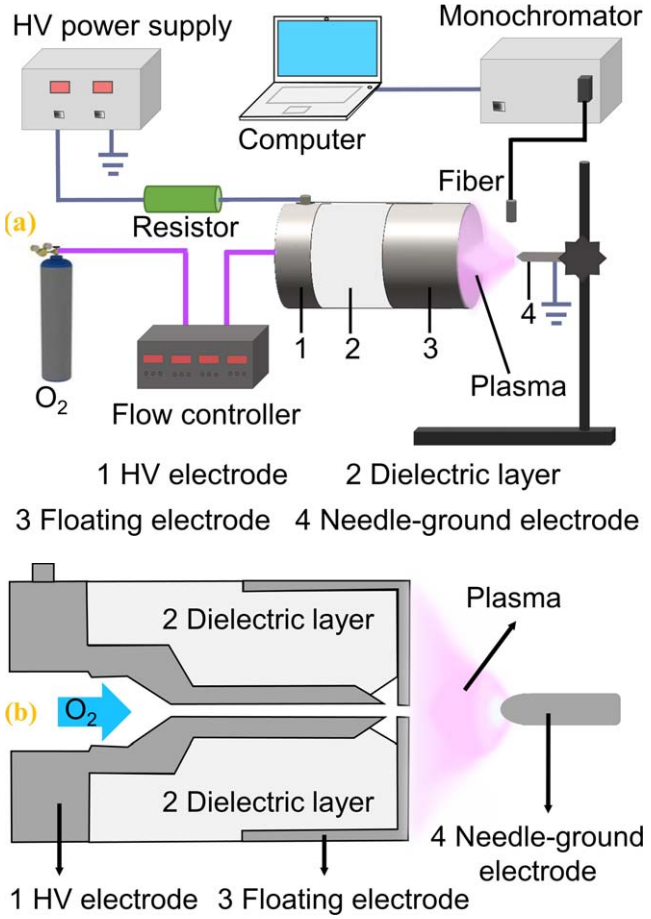

Figure 1. (a) Experiment setup, (b) the section view of plasma reactor in diffuse discharge plasma.

DC. A 3 kΩ ballast resistor is connected in series between the DC power supply and the high-voltage (HV) electrode to stabilize the discharge current. The discharge reactor consists of an HV electrode, a Teflon dielectric layer, an FE and a needle-ground electrode. The sectional view of the reactor is shown in figure 1(b). All of three electrode materials are 304 stainless steel. The inner diameter of the nozzles for both the HV electrode and the FE is 1.5 mm, and the outer diameter of the FE is 30 mm. The thickness of FE is assumed to be 1 mm, and the distance between the nozzle of the HV electrode and the circular hole of the central axis of the FE is 2 mm. The distance between the FE and the needle-ground electrode which is defined as the electrode gap is adjusted in the range of 10–30 mm. In other words, compared with using FE, the electrode gap without FE (the distance between the HV electrode and the needle-ground electrode) is 3 mm larger. In the plasma reactor, the gas inlet is connected with the HV electrode, where high-purity oxygen (99.999%) is injected into the reactor as the plasma working gas, and the gas flow rate, controlled by mass flow controllers, is kept at 0.7 l min^{-1} to generate an oxygen-enriched discharge plasma. An optical fiber collects the photons radiating from the discharge area and transports them to a grating monochromator (Andor SR-750i, the grating groove is 2400 lines mm^{-1} and glancing wavelength is 300 nm) in the optical detection system. A

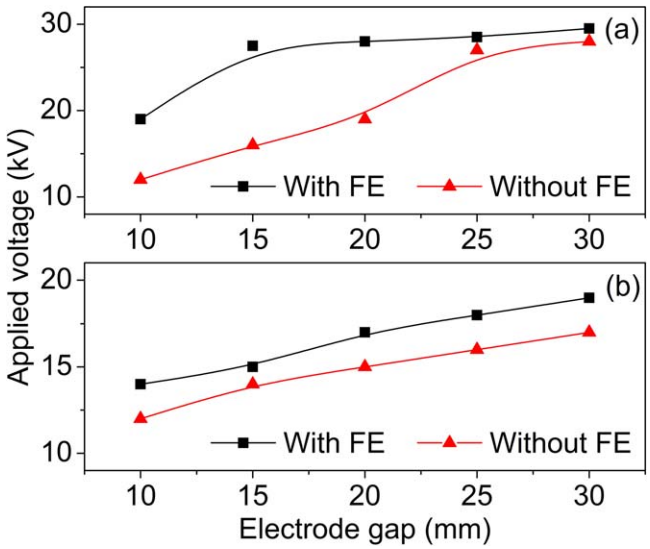

Figure 2. The (a) GST voltage and (b) breakdown voltage of diffuse discharge plasma varies as the functions of electrode gap with or without FE.

CCD camera (Andor Newton DU 940P-BV) is equipped with the grating monochromator for photoelectric conversion and analog signal to digital signal conversion. Finally, the corresponding optical emission spectra (OES) are displayed on a computer. In this paper, the observation zone of all the spectral data collected in the experiment is always located at a position 2 mm away from the tip of the needle-ground electrode in the horizontal axis of the plasma reactor. Moreover, the spectra are measured three times in each experimental condition, and the emission spectra intensities, the vibrational temperature, and the standard deviations are obtained by calculating the rotational temperature separately.

3. Results and discussion

3.1. Electrical properties and discharge image

In order to clarify the effect of the FE on the stability of the discharge, the applied voltage is measured when the discharge starts and the discharge form transfers to spark with and without the FE. We define the above two voltages as breakdown voltage and GST voltage, respectively. Figure 2 shows the GST voltage and breakdown voltage of the discharge varying as function of the length of electrode gap under the gas flow rate of 0.7 l min^{-1}. In the measurement, the location of HV electrode and FE is fixed and the electrode gap is changed from 10 to 30 mm by moving the needle-ground electrode. It is found that both the GST voltage and the breakdown voltage show a rising tendency when electrode gap is increased. The rising tendency is mainly caused by the increase of the value *pd*, which makes the gas breakdown more difficult [28, 29]. The *p* and *d* represent pressure and electrode gap, respectively.

It is also exhibited clearly in figure 2 that the GST voltage and breakdown voltage are higher with the FE than those without FE under the same conditions, and it is noteworthy that compared with non-FE, the range of applied voltage to maintain corona discharge mode and diffuse discharge mode is enlarged with a FE. Especially in the electrode gap of 15 and 20 mm, the applied voltage range of stable discharge is expanded from 14–26 to 15–27.5 kV and from 15–19 to 17–28 kV, respectively. The presence of the FE changes the distribution of the electric field (see figure 4(b)) to be concentrated on the center axis of the high voltage electrode and the needle-ground electrode. In this case, the electric field (see figure 4(a)) between the FE and the needle-ground electrode is similar to the electric field of the pin-plate electrode. In other words, the electric field distributed near the FE is weak while the electric field intensity near the needle electrode is strong. Therefore, ignition or transition of diffuse to spark requires a higher applied voltage when the FE is added [30, 31]. Thus, it is able to maintain a stable discharge (corona discharge and diffuse discharge) over a relatively wide range of applied voltages while the FE is added.

Figure 3 shows the discharge images and corresponding discharge light intensity spatial resolution with FE under the applied voltages of 18 kV, 23 kV and 27 kV. The discharge images are captured by a Cannon EOS 5D Mark IV digital camera. The gas flow rate and the electrode gap are set as 0.7 l min^{-1} and 15 mm, respectively. The MATLAB code [32] is used to analyze the discharge light intensity of the observation area as shown in figure 3(b). It is also can be seen that near the tip of the needle-ground electrode, the discharge light intensity is the strongest under the three applied voltages. As shown in figure 3(a), it is a corona discharge at the tip of the needle-ground electrode as applied voltage is set as 18 kV. The corona gradually transits to a more uniform diffuse discharge, with the area of discharge expanding from the needle-ground electrode to the surface of the FE as the applied voltage increases from 18 to 23 kV. When the applied voltage increases from 23 to 27 kV, the volume of the diffuse discharge area increases obviously and the discharge is more uniform. Especially when the voltage is 27 kV, the plasma can be distributed to the whole bottom of the FE. In addition, the stronger discharge light is observed in the axis direction of the electrode gap, indicating that energetic electrons are more likely to appear in the axis direction of the electrode gap than those in the radial direction during the discharge process. Accordingly, the number of positive ions which are resident in the axis of electrodes is the largest.

3.2. Simulation of electrical field intensity distribution

For the sake of verifying the effect of the FE, we use COMSOL to simulate the electric intensity distribution field before breakdown to understand the initial state of the discharge. According to the actual size and material, the two-dimensional models of plasma reactor with and without FE structure are established. The mesh of the whole model is divided by refinement method. The two electrode structures are simulated by using the electrostatic field module in the software using finite element method. During the calculation, the needle-ground electrode is grounded and the potential of

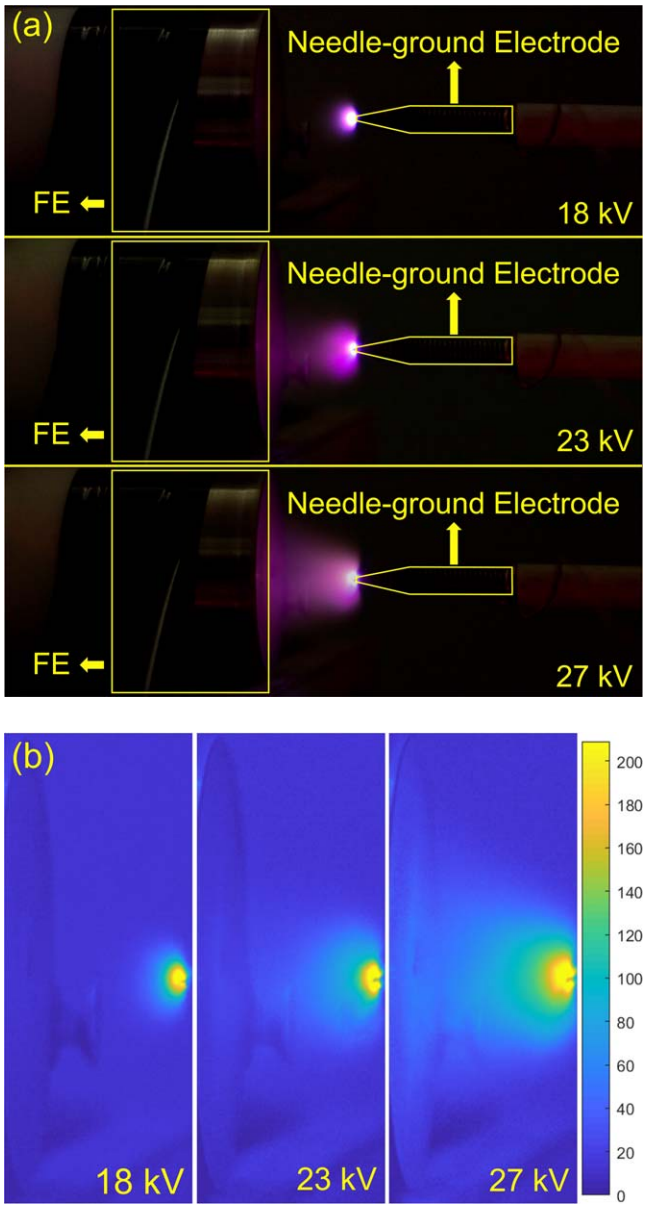

Figure 3. The (a) discharge images and the (b) corresponding discharge light intensity spatial resolution of diffuse discharge plasma with FE. The discharge images are captured by a Canon EOS 5D Mark IV digital camera with an exposure time of 500 ms.

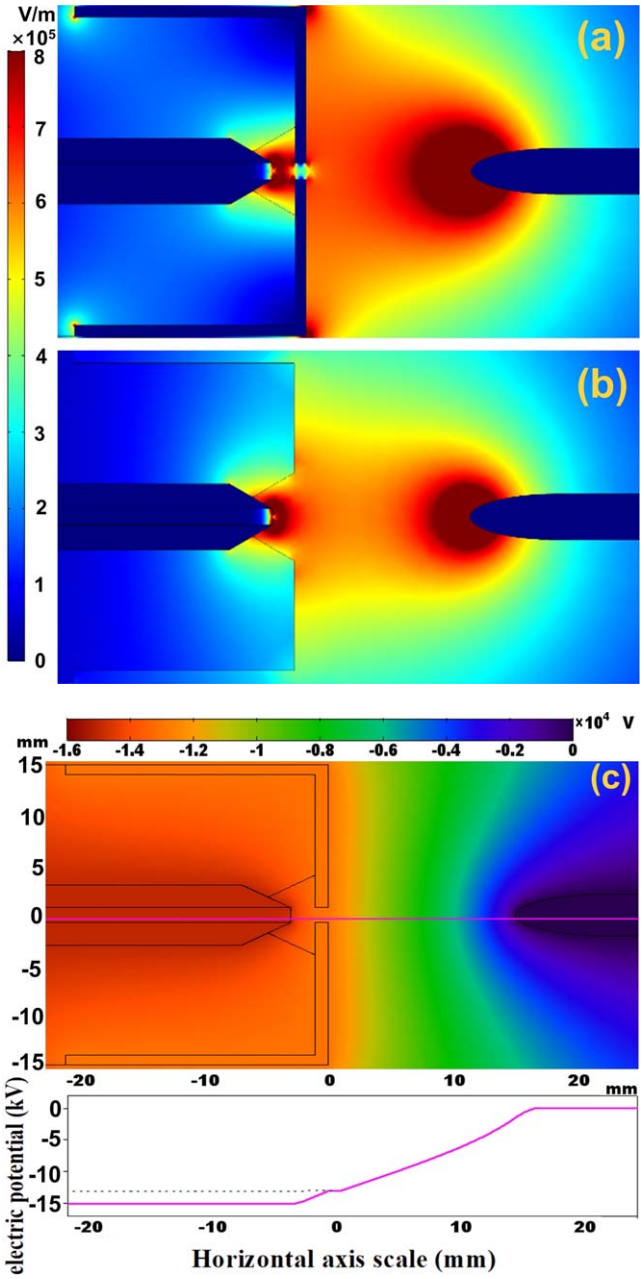

Figure 4. The diagrams of electric field intensity distributions (a) with FE and (b) without FE of diffuse discharge plasma and (c) the spatial distribution of electric potential with FE of diffuse discharge plasma.

the HV electrode is set to the breakdown voltage (−15 kV and −14 kV) of the two structures, respectively. The spatial distribution of the potential near the FE is calculated under the same conditions.

The electric intensity distributions of diffuse discharge plasma with FE and without FE are shown in figures 4(a) and (b), respectively. The electric field intensity distribution is described in section 3.1, and in both of the electrode structures, the strongest electric field is located at the tip of the HV electrode and the needle-ground electrode. Compared with that using FE, the electric field strength near the needle-ground electrode is weaker without FE but it is easier to breakdown and discharge, which is consistent with the results shown in figure 2(b). It is because a lot of input energy is taken up by the discharge between the HV electrode and FE. As can be seen in figure 4(a), although the electric field strength at the needle-ground electrode (3.15×10^6 V m^{-1}) is larger than that of HV electrode tip (1.55×10^6 V m^{-1}), discharge is more likely to occur between the HV electrode and FE because of the small distance between them. According to the study of Liu *et al* [33], it can be speculated that there is discharge between the HV electrode and FE, but it could not be observed directly in the discharge images due to the opaque electrode material.

According to the simulation results of electric potential in figure 4(c), FE forms an equipotential body with an electric potential of −13024 V in the electric field before gas

breakdown. With the increase of applied voltage, gas breakdown is easier to occur between the HV electrode and the FE due to the very small radius of curvature of the HV electrode and the relatively small gap which results in a strong electric field. The electron density increases and the plasma resistance value is very small after the breakdown in the discharge region. Accordingly, the potentials of the FE and the HV electrode are approximately equal. At this point, the HV electrode and the FE can be approximately regarded as a virtual electrode and the above discharges provide seed electrons for the discharge between the virtual electrode and the needle-ground electrode. According to the above description, the electrons emitted by the virtual electrode move towards the needle-ground electrode in the electric field. Due to the strong electric field near the nozzle of virtual electrode shown in figure 4(a), the electrons can obtain high energy in a short distance and collide with the heavy particles to stimulate ionization and thus form electron avalanche [29]. The electron avalanche moves towards the anode with a velocity while positive ions and neutral particles are seen as stationary. A positive corona is then formed at the needle-ground electrode. Under applied voltage of 18 kV, the electric field intensity is not sufficient to sustain ionization at a great distance from the cathode, thus the electron avalanche propagation channel is destroyed and the discharge area does not expand to the virtual electrode. Therefore, it is a corona discharge in 18 kV. As the voltage further increased to 23 kV, corona discharge developed into diffuse discharge by which the electrode gap is bridged as shown in figure 3(a). The diffuse discharge maintains the bridging of the discharge gap while the applied voltage increases from 23 to 27 kV. When the applied voltage increases further, the spark will be observed in the discharge region and a more detailed study has been conducted in the study of Shao *et al* [17].

3.3. Optical emission spectra of the plasma

The OES contain information such as the active species and their radiation types and the vibrational population, which is essential for the diagnosis of plasma characteristics. Figure 5 records the typical OES of the plasma in the ranges of 300–420 nm and 600–800 nm. The applied voltage, electrode gap and gas flow rate are kept at 23 kV, 15 mm and 0.7 l min^{-1}, respectively. The OES mainly consists of the second positive bands N_2(C-B), the first negative bands N_2^+(B-X), the first positive bands N_2(B-A) of N_2, and the line of O(3p–3s, 777 nm). The spectral observation zone is close to the needle-ground electrode, and the O_2 from the HV electrode nozzle has already diffused into the air when it reaches the zone. Therefore, the nitrogen emission spectra can be observed in figure 5(a). In addition, the grating monochromator is equipped with gratings of specific parameters. When some grating slots are used, secondary diffraction lines usually appear at double wavelengths of the spectrum.

The emission spectrum intensity is mainly related to the population and radiation rate of the corresponding particles and it is specifically discussed in the study of Zhao *et al* [34]. Among them, the relevant reactions of the main reactive

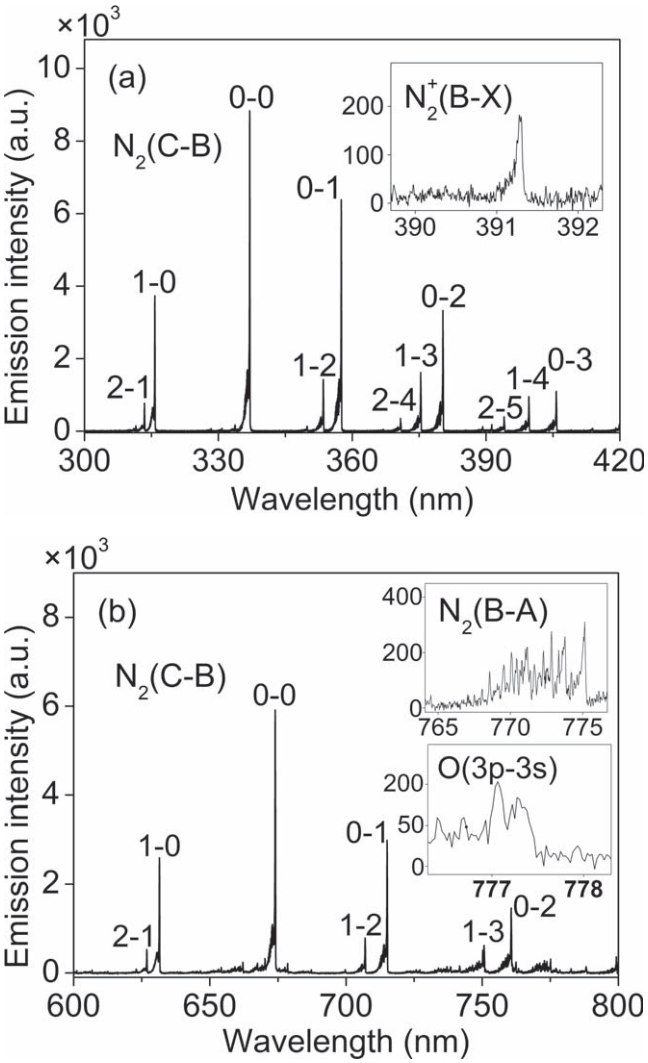

Figure 5. The emission spectra from diffuse discharge plasma with FE in (a) 300–420 nm and (b) 600–800 nm.

nitrogen species are as follows:

$$e + N_2(X) \rightarrow N_2(C) + e \quad (1)$$

$$N_2(C) \rightarrow N_2(B) + h\nu \quad (2)$$

$$N_2(C) + N_2/O_2 \rightarrow \text{products} \quad (3)$$

$$e + N_2(X) \rightarrow N_2(B) + e \quad (4)$$

$$N_2(B) \rightarrow N_2(A) + h\nu \quad (5)$$

$$N_2(B) + N_2/O_2 \rightarrow \text{products} \quad (6)$$

$$e + N_2(X) \rightarrow N_2^+(B) + 2e \quad (7)$$

$$N_2^+(B) \rightarrow N_2^+(X) + h\nu. \quad (8)$$

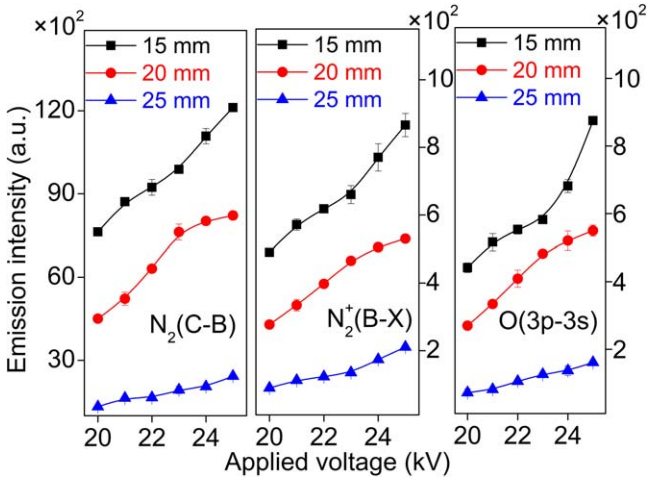

Figure 6. The emission intensities of N_2(C-B, 337.1 nm), N_2^+(B-X, 391.4 nm) and O(3p–3s, 777.4 nm) vary as functions of applied voltages in different electrode gaps with FE.

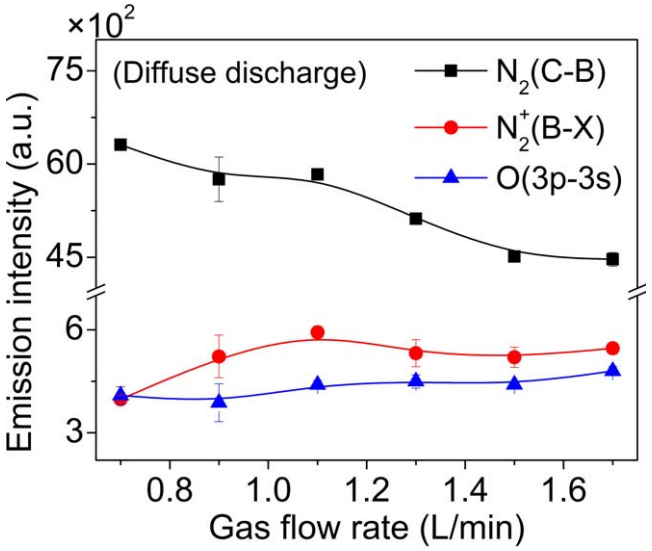

Figure 7. The emission intensities of N_2(C-B, 337.1 nm), N_2^+(B-X, 391.4 nm) and O(3p–3s, 777.4 nm) vary as functions of gas flow rates with FE.

The spectrum of N_2(C-B) in figure 5(b) is the secondary diffraction spectrum. There are two main ways to produce O(3p). One way is that O_2 directly collides with high-energy electrons and is ionized and excited to produce O(3p) (reactions (9)–(11)) [35]. The other way is that the O_2 is ionized by the metastable N_2(A) [36] and then oxygen atom in its product is excited to O(3p) as in reactions (12) and (13) [35]

$$e + O_2 \rightarrow e + O(^3P) + O(^1D) \quad (9)$$

$$e + O_2 \rightarrow e + O(^3P) + O(^3P) \quad (10)$$

$$e + O_2 \rightarrow e + O(^3P) + O(^1S) \quad (11)$$

$$N_2(A) + O_2 \rightarrow N_2(X) + O + O \quad (12)$$

$$e + O \rightarrow e + O(3p^5P). \quad (13)$$

The first way needs a high excitation threshold energy (about 16 eV) which is much higher than that of the N_2(C) product from direct electron collisions with N_2 (about 11 eV) [35, 37]. In another way, most of the products stay in the ground state. Therefore, there is a weak emission intensity of oxygen.

3.4. The effects of applied voltage, electrode gap and gas flow rate on the emission intensity of the plasma

The emission intensity is an indicator of the population of excited particles, which can be generated by one or more channels, and this channel depends on the plasma parameters. Figure 6 shows the emission intensities of N_2(C-B, 337.1 nm), N_2^+(B-X, 391.4 nm) and O(3p–3s, 777.4 nm) as functions of applied voltages in different electrode gaps with the gas flow rate of 0.7 l min^{-1}. It can be clearly seen that the emission spectra intensities of N_2(C-B), N_2^+(B-X) and O(3p–3s) all increase with the applied voltage from 20 to 25 kV. The increasing applied voltage leads to the rise of the electrode field intensity in the discharge region as shown in figure A1, which is the simulation results of electric field intensity in different applied voltages and electrode gaps. With the increasing electrode field intensity, more energetic electrons are generated in the discharge region [38]. Then they excite upper states of radiation transitions, resulting in more active particles. Therefore, the intensities of the corresponding emission spectra of N_2(C-B), N_2^+(B-X) and O(3p–3s) increase with the rising applied voltage accordingly.

As shown in figure 6, the emission intensity of above reactive species is much stronger in smaller electrode gap. The simulation results of electric field intensity as a function of applied voltage at electrode gaps of 15 mm, 20 mm, and 25 mm are shown in figure A1. With the increase of the electrode gap, the electric field intensity decreases significantly. Therefore, at the same applied voltage, the average electric field in a bigger electrode gap is weaker. Thus, there are fewer active particles produced, and the emission intensities of the above active particles significantly decrease with the electrode gap increases from 15 to 25 mm.

The effects of gas flow rate on the emission spectra intensities of N_2(C-B), N_2^+(B-X) and O(3p–3s) with FE are all shown in figure 7. The applied voltage and electrode gap are kept at 23 kV and 20 mm, respectively. It is clearly shown that the emission intensity of N_2(C-B) decreases with increasing gas flow rate while the variations of the emission intensities of N_2^+(B-X) and O(3p–3s) are almost independent of the gas flow rate. With the increase of oxygen flow rate, the number of O_2 molecules in the spectral acquisition zone of discharge region increases while the number of N_2 molecules decreases. O_2 is an electronegative gas, which can absorb electrons and reduce the electron density in the plasma. This allows fewer excited particles N_2(C) and O(3p) to be produced. As a result, the emission intensity of N_2(C-B) shows a clear downward trend and the emission intensity of O(3p–3s) does not change significantly. N_2^+(B) is mainly derived from energetic electron direct collision excitation, which requires the energy of the energetic electrons to be about at least 18.7 eV [35]. The N_2^+(B) is considered a symbol of unstable discharge mode accordingly. While the gas flow rate has

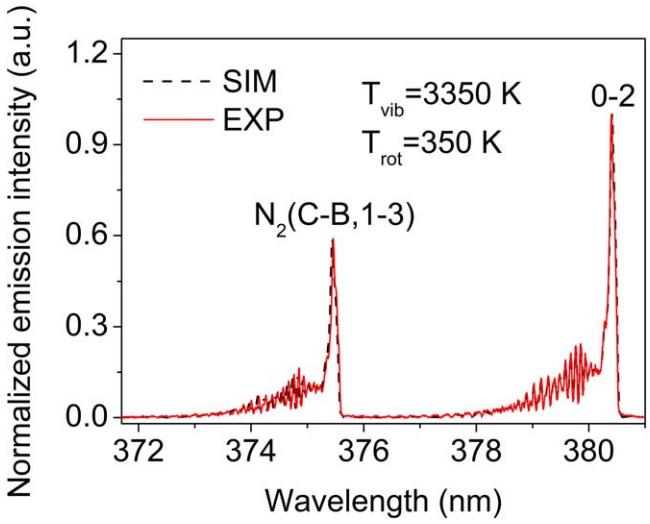

Figure 8. Plots of the simulated and measured spectra of N_2(C-B, 371–382 nm) under the electrode gap of 15 mm with FE.

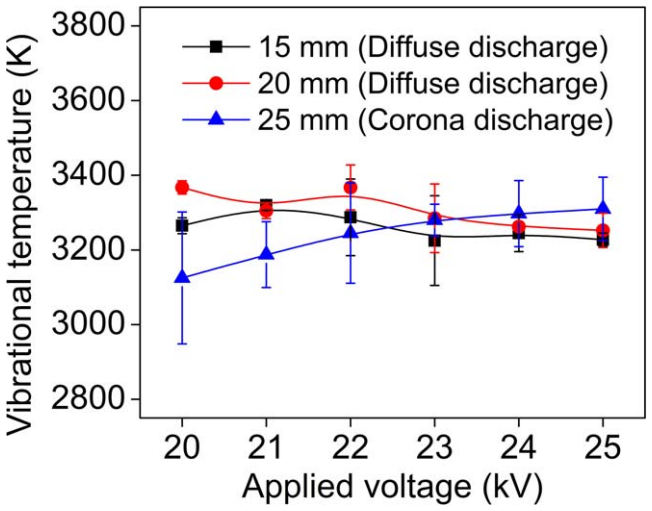

Figure 9. The effect of applied voltage on vibrational temperature of the diffuse discharge plasma with FE at different electrode gaps.

almost no effect on the discharge mode, and there is still no filamentous discharge caused by the contraction of the discharge channel (see figure A2). Therefore, the number of energetic electrons whose energies reach 18.7 eV does not change significantly, as well as the N_2^+(B) that produced. Thus, there is no obvious upward trend in the emission intensity of N_2^+(B-X).

3.5. Characteristics of rotational temperature and vibrational temperature

Rotational temperature and vibration temperature are important parameters of plasma, which can directly affect the chemical reaction rate of the plasma and the surface characteristics of target materials. The vibrational temperature reflects the existence of energy in the excited state of molecular vibration, and the higher vibrational temperature can effectively promote the chemical reaction in plasma. The population of the rotational levels in molecular species is described by rotational temperature. SPECAIR can accurately simulate a variety of molecular transitions including NO, N_2, N_2^+, OH and CO, as well as atomic lines of N, O and C [39]. The vibrational and rotational temperatures of N_2 molecules are calculated by this method and the original spectra are normalized by SPECAIR before computation. Figure 8 shows the measured and simulation spectra of N_2(C-B, 371–382 nm) in the diffuse discharge plasma under the applied voltage of 23 kV and the gas flow rate of 0.7 l min^{-1}. In atmospheric plasma, the rotational energy and kinetic energy of molecules are balanced by frequent collisions between heavy particles due to the small energy and gap of rotational energy levels of molecules [40]. Therefore, it can be considered that the gas temperatures are equal to the rotational temperature of N_2. From the results in figure 8, it is clear to see that the simulated spectrum fits well with the experimental one. The result demonstrates that under these conditions the vibrational and rotational temperatures of N_2(C) in diffuse discharge plasma are 3350 ± 20 K and 350 ± 10 K respectively, which means that the gas temperature of diffuse discharge plasma is 350 ± 10 K that is close to room temperature.

Figure 9 shows the variations of the vibrational temperature of atmospheric diffuse discharge plasma when the applied voltage increases in different electrode gaps under the gas flow rate of 0.7 l min^{-1}. The discharge gap is bridged completely when the electrode gap is set to 15 and 20 mm, and it is not bridged completely when the electrode gap is set to 25 mm. Therefore, the vibrational temperature has different trends in the three-electrode gap as the applied voltage increases, which is discussed separately in [41]. The vibrational temperature, which indicates electron energy, is reduced when the applied voltage is increased at the electrode gaps of 15 and 20 mm. Due to the complete breakdown of electrode gap, as the applied voltage rises, the current density and conductivity of the discharge area increase, while the discharge current increases [41]. As a result, the reduced electric field that reflects the average electron energy is reduced [28]. On the other hand, as the applied voltage increases, more energy is transferred from the heating electron to the heavy neutral particle, which is part of the reason why the vibration temperature tends to decrease. Similarly, compared with the electrode gap of 20 mm, the discharge current and average electron energy of 15 mm electrode gap are smaller, thus the vibrational temperature is lower [41, 42].

For the electrode gap of 25 mm, with the increase of the applied voltage, the discharge is concentrated in a small area near the needle-ground electrode and the reduced field intensity increases [43, 44]. The electron can obtain higher energy and the discharge zone is small at the electrode of 25 mm. Thus the mean electron energy and the vibrational temperature increase with the increase of voltage, as shown in figure 9.

The rotational temperature as a function of applied voltage at different electrode gaps in the diffuse discharge plasma when the gas flow rate is 0.7 l min^{-1}, is shown in figure 10. With the rise of applied voltage, the rotational temperature obtained by SPECAIR software increases in

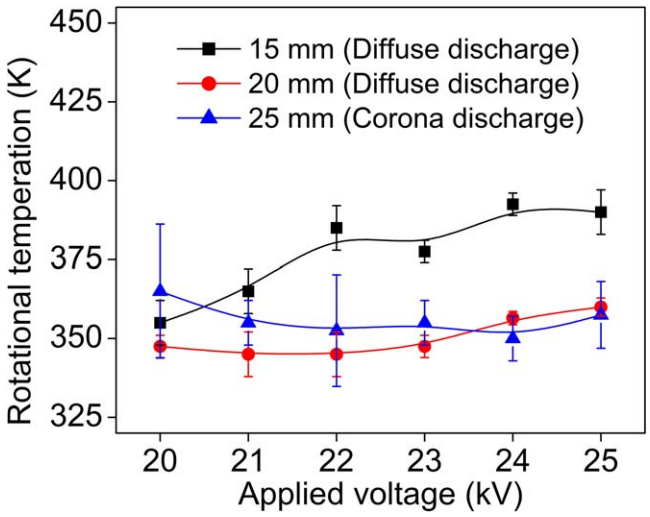

Figure 10. The effects of applied voltage on the rotational temperature of the discharge plasma with FE at different electrode gaps.

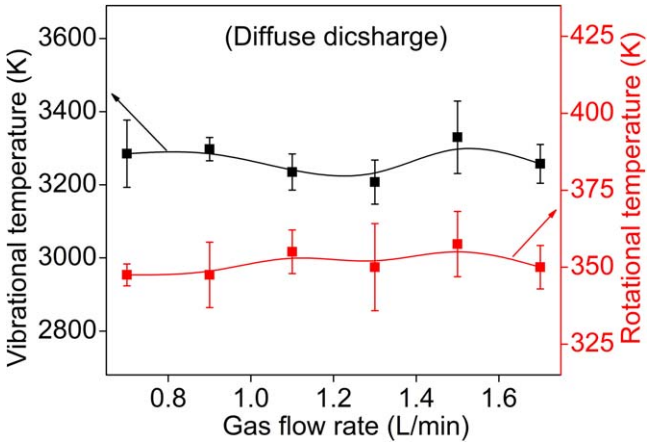

Figure 11. The effects of gas flow rate on the vibrational temperature and the rotational temperature of the diffuse discharge plasma with FE.

electrode gaps of 15 and 20 mm. When the applied voltage increasing, the plasma power increases and the rise of energy injected into discharge region makes the collision between electrons and heavy particles more frequent, which makes the rotational temperature rise and the Joule heating effect become more obvious [45]. Thus, the rotational temperature with the electrode gap of 15 mm is higher and the rising trend is more obvious than that in 20 mm.

As can be seen from figure 10, the rotational temperature curves slightly decrease when the applied voltage is increased at the electrode gap of 25 mm. It is caused by the short displacement of gas molecules and ions in the small discharge region which results in a unobvious heating effect. In addition, it can be observed in figures 9 and 10 that the curve error bar with electrode gap of 25 mm is relatively more obvious. This is because the increase of electrode gap reduces the area of the discharge region, which reduces the signal to noise ratio of the emission spectrum.

The effects of gas flow rate on the vibrational temperature and the rotational temperature are shown in figure 11. The applied voltage and electrode gap are kept at 23 kV and 20 mm, respectively. The gas flow rate varies over a relatively small range. Thus, it can be seen that the vibrational temperature and the rotational temperature are almost unaffected by the gas flow rate.

4. Conclusions

In this paper, an atmospheric pressure large-area diffuse discharge plasma is successfully obtained in an open oxygen-enriched environment by using a specially designed FE and the characteristics of the discharge plasma are studied in diagnosis. The effects of FE on the GST voltage and breakdown voltage are investigated by combining the simulated electrostatic field before breakdown. These findings emphasize that FE can increase the GST voltage and breakdown voltage by altering the electric field distribution, and it can effectively broaden the applied voltage range of stable discharge (corona or diffuse discharge). It is shown that the FE can inhibit GST to a certain extent, which is beneficial to maintain the stability of the discharge. Meanwhile, the emission spectrum of the discharge plasma with the FE is collected, and the vibrational temperature and rotational temperature of N_2(C-B) are calculated through it. These data revealed that the emission intensities of N_2(C-B), N_2^+(B-X) and O(3p–3s) rise with increasing applied voltage and slow down with increasing electrode gap. For the vibrational temperature, there is a slight tendency for the vibrational temperature to decrease in the diffuse discharge mode at electrode gaps of 15 and 20 mm with the increased applied voltage. At the electrode gap of 25 mm, the discharge mode is corona, and the vibrational temperature rises when the applied voltage is increased. The rotational temperature, which is considered to be equal to the gas temperature, increases with the increase of applied voltage at the electrode gap of 15 mm and it implies that the thermal effect is more evident in the small electrode gap. In conclusion, under oxygen-rich conditions, a large area of diffuse discharge plasma with moderate gas temperature and abundant active particles can be obtained by using the FE structure. This provides important value for material surface treatment and other applications.

Acknowledgments

This work is supported by National Natural Science Foundations of China (Nos. 11965018, 51977023 and 52077026), the Science and Technology Development Fund of Xinjiang Production and Construction of China (No. 2019BC009), the Fundamental Research Funds for the Central Universities of China (No. DUT21LK31), the Key Laboratory Fund of National Defense Science and Technology of China (No. 6142605200303), Science and Technology Plan Project of the Ninth Division of the Crops of China (No. 2021JS003).

Appendix

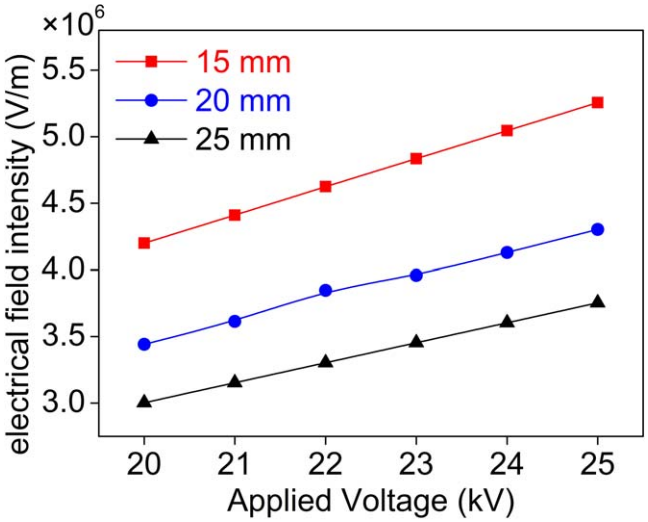

Figure A1. The electric field intensity varies as a function of applied voltage when electrode gaps are 15 mm, 20 mm, 25 mm, respectively. The selected position of the electric field intensity is the tip of the needle-ground electrode (on the central axis of the plasma reactor).

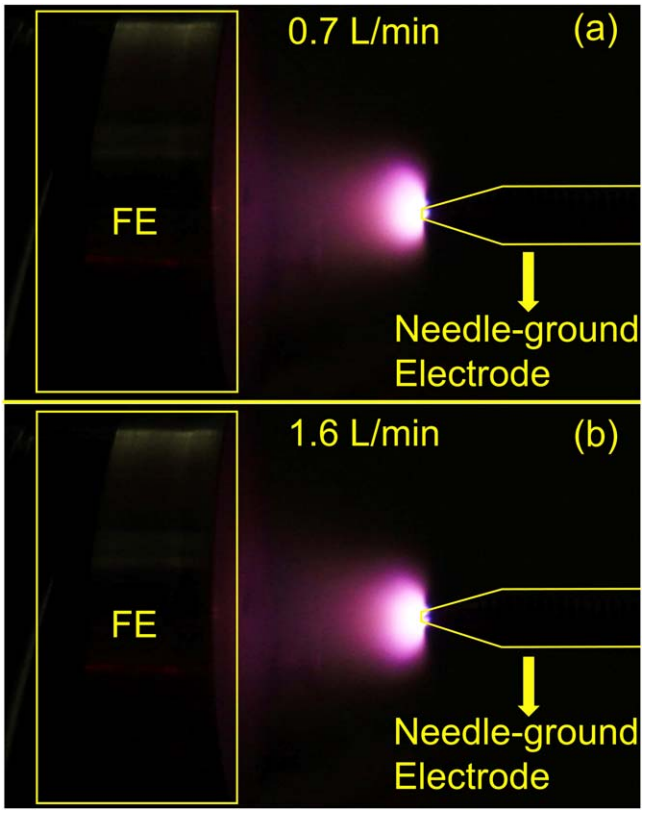

Figure A2. The discharge images of diffuse discharge plasma with FE under the gas flow rate of 0.7 l min^{-1} and 1.6 l min^{-1}. The discharge images are captured by a Canon EOS 5D Mark IV digital camera with an exposure time of 500 ms. The electrode gap is 15 mm and the applied voltage is 23 kV.

References

[1] Semmler M L *et al* 2020 *Cancers* **12** 269
[2] Borges A C *et al* 2021 *Appl. Sci.* **11** 1975
[3] Qin H B *et al* 2022 *J. Hazard. Mater.* **430** 128414
[4] Pankaj S K *et al* 2014 *Trends Food Sci. Technol.* **35** 5
[5] Misra N N *et al* 2011 *Food Eng. Rev.* **3** 159
[6] Misra N N *et al* 2016 *Trends Food Sci. Technol.* **55** 39
[7] Yuan H *et al* 2018 *Surf. Coat. Technol.* **344** 614
[8] Desmet T *et al* 2009 *Biomacromolecules* **10** 2351
[9] Wang H L *et al* 2022 *Chem. Eng. J.* **431** 133858
[10] Bogaerts A *et al* 2020 *J. Phys. D: Appl. Phys.* **53** 443001
[11] Wang R X *et al* 2022 *Plasma Chem. Plasma Process.* **42** 303
[12] Wang H L *et al* 2021 *J. Phys. D: Appl. Phys.* **54** 025202
[13] Park C S, Kim D Y and Kim S O 2014 *IEEE Trans. Plasma Sci.* **42** 2490
[14] Wu S Q *et al* 2017 *Plasma Process. Polym.* **14** 1700112
[15] Kogelschatz U 2002 *IEEE Trans. Plasma Sci.* **30** 1400
[16] Huo W G *et al* 2014 *Phys. Plasmas* **21** 053505
[17] Shao T *et al* 2013 *J. Appl. Phys.* **113** 093301
[18] Zhang S *et al* 2019 *Spectrochim. Acta* A **207** 294
[19] Shi J J and Kong M G 2006 *Phys. Rev. Lett.* **96** 105009
[20] Shi J J, Liu D W and Kong M G 2006 *Appl. Phys. Lett.* **89** 081502
[21] Shi J J, Liu D W and Kong M G 2007 *Appl. Phys. Lett.* **90** 031505
[22] Kanazawa S *et al* 2006 *Plasma Process. Polym.* **3** 692
[23] Hu J T *et al* 2013 *Phys. Plasmas* **20** 083516
[24] Roman F, Cooray V and Scuka V 1996 *J. Electrostat.* **37** 67
[25] Divya Deepak G 2022 *Eur. Phys. J. Appl. Phys.* **97** 39
[26] Divya Deepak G *et al* 2017 *Rev. Sci. Instrum.* **88** 013505
[27] Zhu T H *et al* 2022 *J. Anal. Appl. Pyrolysis* **164** 105529
[28] Yang D Z *et al* 2012 *Plasma Sources Sci. Technol.* **21** 035004
[29] Raizer Y P 1991 *Gas Discharge Physics* (Berlin: Springer)
[30] Zhang L *et al* 2019 *Nanomaterials* **9** 1381
[31] Liu C, Fridman A and Dobrynin D 2019 *J. Phys. D: Appl. Phys.* **52** 105205
[32] Yuan H *et al* 2017 *Plasma Sci. Technol.* **19** 125401
[33] Liu W Z *et al* 2017 *Europhys. Lett.* **118** 45001
[34] Zhao Z L *et al* 2016 *Spectrochim. Acta* A **161** 186
[35] Li Y *et al* 2020 *Plasma Sources Sci. Technol.* **29** 055004
[36] Herron J T 1999 *J. Phys. Chem. Ref. Data* **28** 1453
[37] Li Y *et al* 2021 *J. Phys. D: Appl. Phys.* **54** 245206
[38] Zhao Z L *et al* 2017 *Plasma Sci. Technol.* **19** 064007
[39] Laux C O *et al* 2003 *Plasma Sources Sci. Technol.* **12** 125
[40] Luo S Q, Denning C M and Scharer J E 2008 *J. Appl. Phys.* **104** 013301
[41] Shao T *et al* 2011 *IEEE Trans. Plasma Sci.* **39** 1881
[42] Zhang L *et al* 2014 *J. Appl. Phys.* **116** 113301
[43] Liu F *et al* 2006 *Plasma Chem. Plasma Process.* **26** 469
[44] Yang D Z *et al* 2010 *J. Phys. D: Appl. Phys.* **43** 455202
[45] Kunhardt E E 2000 *IEEE Trans. Plasma Sci.* **28** 189